



Curved Beam Based Model for Piston-Ring Designs in Internal Combustion Engines: Working Engine Conditions Study

Mohamed Aziz Bhouri and Tian Tian Massachusetts Institute of Technology

Citation: Bhouri, M.A. and Tian, T., "Curved Beam Based Model for Piston-Ring Designs in Internal Combustion Engines: Working Engine Conditions Study," SAE Technical Paper 2018-01-1277, 2018, doi:10.4271/2018-01-1277.

Abstract

A new multi-scale curved beam based model was developed for piston-ring designs. This tool is able to characterize the behavior of a ring with any cross section design. This paper describes the conformability and ring static twist calculation. The conformability part model the static behavior of the ring in working engine conditions. The model employs the computation scheme that separates the meshing of the structure and local force generation. Additional to the conventional static ring-bore conformability analysis, the conformability model is designed to examine ring-bore and ring-groove interactions in a running

engine under varying driving forces and localized lubrication conditions. We made improvements on the way to handle the effects of the radial temperature gradient compared to the existing models. Examples are given on the effects of ring rotation on the interaction of the ring and a distorted bore as well as the change of local lubrication conditions. Ring static twist calculation was also included to provide necessary input for 2D models. The present model can become a viable ring design tool revealing not only static ring behavior but also the distribution of the clearance and force between ring and bore as well as groove under the dynamic situation of an engine cycle.

Introduction

Ring design include two categories: material and geometry designs. Geometry design for top two rings relies on three key elements, namely ring free shape, its cross-section and its running surface profile and these elements determine the interaction of the ring with the liner as well as with the piston groove [1, 2].

Considering only dry contact and oil lubrication, the ring-liner interaction is determined by the ring geometry and the bore shape. Due to the thermal expansion and cylinder head bolting, the bore is not perfectly circular and is subject to distortions. At the same time, ring geometry is rarely found as designed initially, mainly because of the plastic deformation during the manufacturing stages. Thereby, it is crucial in practice to know the contact force based on the ring geometry and bore shape.

There are multiple analytical works on ring bore conformability. Timoshenko and Lessell [3] presented a solution for a circular ring conforming to a circular bore, where they developed a formula for a variable wall thickness of a rectangular cross-section ring in order to achieve a uniform contact pressure on a circular bore. Sun [4] modeled the ring as a curved beam with in-plane elastic, gas and thermal loads at a steady state within a distorted bore. The identification of the bore distortion as a potential source of oil consumption [5, 6, 7] triggered several studies. An analytical criterion to compute the maximum admissible bore distortion was carried out by Mueller [8]. Dunaevsky used a similar analytical approach

and statistical treatment of bore distortion in order to determine different bore distortion limits [9, 10, 11, 12, 13]. Later on, Tomanik suggested a new conformability criterion based on experimental measurement of ring conformability limits [14, 15]. Using ANSYS, Ma et al. [16] developed different independent models (gap model, cable model and thermal liner model) to study ring-liner conformability and also the effect of thermal stress.

Most of these models rely on the small displacement assumption. However, the ring shape changes significantly when the ring is closed from its free shape into the bore and hence that assumption is no longer valid and would cause notable errors. Besides, all the existing models were developed for ring with symmetric cross-section, while rings could also be designed to have asymmetric cross-section in practice. This asymmetry will affect the ring behavior since it will introduce linear and angular displacement in all directions, which will affect ring-bore and ring-groove interactions.

Finite element methods have been used to model the structural behavior of the ring and its interaction with the cylinder [17, 18, 19, 20]. However most of the existing structural models are based on straight beam model which has some limitations as the discontinuity of physical properties at the nodes of the finite element grid such as the curvature in addition to the large number of elements needed to reach sufficient accuracy which hamper the computation cost of these models.

It is of utmost importance for ring manufacturers to have an analytical tool that determines the required ring free shape

which will provide the desired ring-bore and ring-groove conformability and the required interactions. Besides, taking into account ring gap location, thermal moment, piston secondary motion, gas pressures and the different lubrication cases is of practical interest since it models the ring within engine working conditions. Prescott et al. [21] has developed an analytical solution for the free shape of a ring with constant rectangular cross-section that will give a uniform ring-bore contact pressure. That solution is quoted as the basis of piston ring design. However, this approach uses small displacement approximation when modeling ring closure from its free shape, which does not give accurate estimation since that condition is violated and that tool does not determine the ring free shape for any arbitrary contact pressure distribution.

In order to control oil transport more efficiently, compression rings are generally designed to have static twist angles once inserted into the piston and cylinder. This is accomplished by designing asymmetric cross-section. It is of practical interest for ring designers to have an analytical tool that determines the ring static twist based on its design which will facilitate the iterative design process needed to obtain the desired static twist. Few published studies on the ring static twist calculation are available. Dunaevsky et al. [10, 11, 22] have developed models to calculate the ring static twist. However, the boundary conditions used in these models do not really correspond to the engine applications.

Piston rings have been studied extensively in order to characterize their performance in terms of conformability which plays a critical role in determining oil consumption, gas blow by and friction. Yet no complete ring design tool based on curved beam model has been developed. A straight beam based ring design tool was developed by Liu [23]. However, this modeling does not include oil lubrication, variable oil supply along the circumference and non-zero gap effects.

Conformability should also be studied with the ability of modelling working engine conditions including the different lubrication cases, the gas pressure effect along with the groove and bore distortion and thermal moment effect. Besides, non-zero ring gap and variable oil distributions and gas pressures along the circumference should be modeled since these conditions can be encountered in working engine conditions.

As proven by Baelden [24, 25], curved beam model resolved several issues existing in the straight beam model such as discontinuities of quantities of bending moment and curvature, and the singular behavior of the ring gap that can be studied with a higher degree of confidence. Hence, developing a static twist under fixed ID/OD constraint based on curved beam model is essential to conceive a complete ring design tool based solely on that modelling that allows us to reach a better accuracy with less computation cost than the straight beam model.

This work is focusing on the top two rings but the methodology and the RDT developed can be extended to study the OCR.

Our model relies on a multi-scale meshing which is able to solve the ring structural deformation of the piston ring using a coarse mesh but considers the different interactions with the liner and piston on a finer contact grid. This method allows efficient coupling of structural deformation of the ring

and contact forces at the ring-liner and ring-groove interfaces which occur at different length scales. As a result, contact and gas forces can be simulated taking into account relevant factors such as bore distortion or piston tilt.

Conformability Model Development

Curved Beam Finite Element Model of Piston Rings

Radial bore distortions are typically of the order of $100 \mu m$, while ring's radial deformations from its free shape are of the order of $1 mm$ and its length is in the order of tens of millimeters. However, ring-liner and ring-groove contact forces depend on the clearances which are within sub-micron level and the on boundary conditions like fuel-lube interaction and bridging which include length scales around $10 \mu m$ and even lower. Therefore, the classic straight beam description is not able to respect the local force generation and provide an accurate description of the structural deformation physics.

To address this problem and to couple ring deformations and its contact interaction with the piston and cylinder despite their different length scales, a dual grid curved beam finite element method was developed by Baelden [24, 25] first and then used by Y. Liu [26, 27, 28] to successfully assemble a multi-scale-length ring pack model that provides an accurate description of a cycle model and all the relevant mechanisms taking part in it within a reasonable computation cost.

This curved beam finite element method takes advantage of the dual grid used for the ring's deformations and the contact force based on the typical length scales they rely on. Ring structural deformations are solved with sufficient accuracy using a coarse structural mesh and local interactions are studied based on a much finer grid. Thanks to this separation, this method is able to address the problem mentioned above by handling different length scales at the same time.

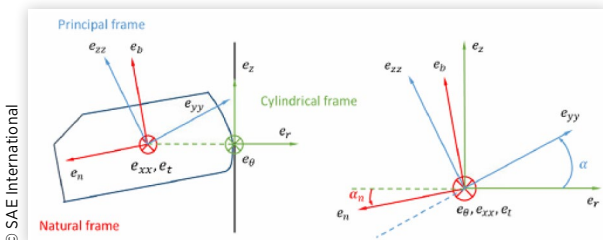
The radial and axial displacements of the ring neutral axis are interpolated using 5th order Hermite polynomial spline in order to guarantee the continuity of these displacements up to their second derivatives. Hence, under the small displacement assumption, the continuity of the curvatures corresponding to the radial and axial displacement, which is the key variable for bending, follows as we can see in equations (1)-(3) where R is the nominal ring radius, y the radial displacement, z the axial lift and α the angle between the principal frame and cylindrical one as shown in Figure 1.

$$\kappa = \frac{1}{R} - \frac{y + y''}{R^2} \quad (1)$$

$$\kappa_{yy} = \kappa \cos\left(\alpha + \frac{z''}{R}\right) \quad (2)$$

$$\kappa_{zz} = \kappa \sin\left(\alpha + \frac{z''}{R}\right) \quad (3)$$

FIGURE 1 Ring principle frame (blue), Natural frame (red) and Cylindrical frame (green)



The expressions of the different bending moments and twist moment are given below (4)-(6) and show the dependence on the ring coordinates and their derivatives, where E is ring Young modulus, I_{zz} its cross section moment of inertia in plane, I_{yy} its cross section moment of inertia out of plane, J_t its torsion factor and G its shear modulus. κ_{yy0} and κ_{zz0} refer to the ring free-shape curvature corresponding to the radial and axial projections.

$$M_{zz} = EI_{zz} (\kappa_{yy} - \kappa_{yy0}) \quad (4)$$

$$M_{yy} = EI_{yy} (\kappa_{zz} - \kappa_{zz0}) \quad (5)$$

$$M_\theta = GJ_t \left(\frac{z' - Ra'}{R^2} \right) \quad (6)$$

Since the twisting moment depends on the first derivative of the twist angle and its second derivative does not appear in the expressions of the different moments, a 3rd order polynomial interpolation is sufficient and requires only ring twist and its first derivative at the nodes.

Next we apply Hamilton's principal by considering Euler-Lagrange equations and introduce an intermediate state in our simulation which corresponds to closing the ring from its free-shape to the circular bore. During that process, the small displacement assumption is violated and hence the simplified expressions of the curvature and moments provided above are not valid anymore. The closing process is considered by taking into account the load required to close the ring from its free shape as an initial one.

The finite element equation of motion is derived for each element. Then, the different element matrices and vectors are assembled to obtain the finite element equation of the complete ring with global matrices.

We apply the curved beam finite element model to study the ring conformability with the groove and the liner. We also used the method introduced to handle large displacement when closing the ring starting from its free shape to its nominal radius. As proved in L. Liu works [19, 20, 23] and in Y. Liu thesis [26], many useful analyses can be carried out without including ring's dynamics. This study includes contact force distribution relations, ring interaction with a distorted bore and ring interaction with gas pressures. We also include in our work the effect of oil lubrication on the groove flanks and liner, the non-zero gap effect and the modeling of the thermal moment introduced by the temperature gradient between the ring's inner diameter (ID) and outer diameter (OD).

Force Analysis

In engine cycles, the piston rings have different forces applied on them. Besides inertia, when assembled into piston, the top two rings are closed from their free shape and as described in the previous section, the change of curvature and torsion of their neutral axes create internal stress which is considered in our model as initial force. Pressured gas flows around the ring pack system and contributes to pressure force in both radial and axial directions. The liner provides dry or hydrodynamic contact force in the radial direction and friction force in the axial one. The ring-groove interaction includes dry contact force, oil pressure force due to squeezing and also gas pressure force if gas flows through the ring-groove clearance.

Ring-liner force includes two different contact models. One of them is the dry contact force which is derived from Greenwood and Tripp work on rough surfaces contact [29]. More precisely we use the simplified formulation derived by Hu [30]. The other force is the hydrodynamic pressure and for which we differentiate between the fully flooded and the partially flooded conditions. Different mechanisms determine the oil supply to the top two rings. The oil film thickness on the liner, in most of the areas traveled by the top two rings, is controlled by the oil control ring. In this case, the oil supply is partially flooded and the deterministic correlations of the top two rings developed by Chen [31, 32] can be used to determine the hydrodynamic pressure and the shear stress between the top two rings and the liner. Oil supply to the top two rings does not always come solely from the oil film left by the oil control ring. In some cases, around the top or bottom dead centers of the liner, bridging may occur and this brings additional amount of oil from the piston to the liner. This extra oil bypasses the oil control ring and encounters directly the top two rings. Therefore, the boundary condition of the top two rings changes to fully flooded. Bridging brings an additional amount of oil with a thickness of the order of $10 \mu\text{m}$ which exceeds the correlating range of the partially flooded condition. Besides, the large oil film thickness implies that the surface roughness does not have significant effect anymore. Therefore, we can determine the hydrodynamic force using Reynolds equation for a given ring profile and a smooth liner as developed by Liu Y et al. [28].

Ring-groove interaction includes the asperity contact force, oil pressure force due to squeezing, hydrostatic force and gas pressure force. We assume that there is a uniform oil layer on both groove flanks. This assumption lets us obtain a qualitatively accurate estimation of the acting force from oil squeezing effect. For the ring-groove geometry, our tool allows for piston tilting and piston offset. As for the ring-liner interaction, the ring-groove dry contact is modeled using the simplified formulation of the Greenwood and Tripp pressure contact model [29, 30]. As suggested by Tian [33, 34], provided that the oil film thickness is on the order of a few microns, the oil flow between the ring and the groove flanks has Reynolds number on the order of one and the angle between the ring and the groove is on the order of 0.01 rad . Therefore, we can apply the Reynolds equation. Tian also pointed out that the ring's moving away from the groove starts from a certain point and then gradually extends to the entire part of the ring. Thus, the possibility of suction or negative pressure is negligible. The

ring-groove interacting area is not always the same as the ring-oil contact area. Thus, gas will fill in the space between the ring and the oil film generating hydrostatic pressure force. Finally, when the ring-groove clearance is larger than the oil film thickness on the groove, gas will flow driven by pressure difference. As studied by Tian [33, 34], this gas flow through the ring-groove clearance can be treated as laminar flow.

Thermal Moment

In general, during engine operation, the temperature increase of the ring is higher at ring ID than at ring OD, creating a temperature gradient in the radial direction. This temperature difference tends to decrease the curvature of the ring. Cheng et al. [35] have developed a three-dimensional model for ring-bore contact that considers temperature gradient at real operating conditions. By solving a steady-state thermal conduction problem within the ring with convective boundary conditions, their finite element analysis is used to calculate the resulting temperature distribution and thereafter the additional thermal load. Along with validating their model with experiments, they showed the importance of temperature gradient effect on the ring liner interactions and the significant impact of temperature compensation on the separation gap size at the ring tips. Piston rings producing tip contact concentration under thermal stresses were first studied by Mierbach [36] and his results were used by L. Liu [23]. In that model, the effect of thermal stresses on ring shape was considered equivalent to the effect that would result from applying a bending moment on the ring tip. That explains the high contact pressure and thus the heavy wear that usually occurs around the ring tips. In our study, we compared that modeling to the introduction of the thermal effect along the whole ring, since the temperature gradient between the ID and OD exists all around the ring and not only at the tip. That comparison is given in the results part. To do so, we modified the curvature of the ring appropriately so that we consider the thermal effect before modeling the ring's conformability within the piston, which is different from L. Liu [23] model where he consider the thermal moment as an external force acting only at the ring tips.

The bending moment along the e_{zz} direction is proportional to the curvature change in the e_{yy} direction.

$$M_{zz} = EI_{zz} (\kappa_{yy} - \kappa_{yy0}) \quad (4)$$

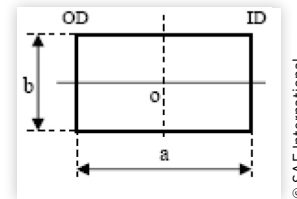
Therefore we modify the ring's free shape curvature κ_{yy0} , which is an input to our model by subtracting the term corresponding to the thermal moment effect which gives us the following new ring curvature to consider:

$$\kappa_{yy0}^n = \kappa_{yy0} - \frac{M_t}{EI_{zz}} \quad (5)$$

M_t is the thermal moment caused by the non-uniform temperature change in the radial direction. For a ring with a rectangular cross-section as shown in Figure 2, the thermal moment can be expressed by the following equation:

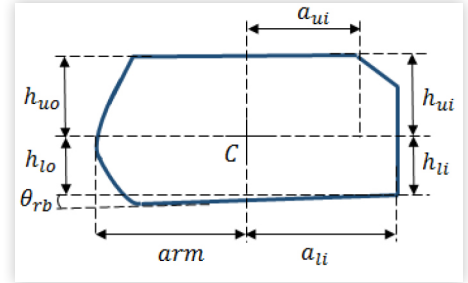
$$M_t = \int_{-\frac{a}{2}}^{\frac{a}{2}} y \alpha_T \Delta T(y) E b dy \quad (6)$$

FIGURE 2 Rectangular ring-cross section dimensions



© SAE International

FIGURE 3 Ring-cross section dimensions



© SAE International

$\Delta T(y)$ represents the temperature change at the radial location y compared to the design temperature at that location. α_T is the ring thermal expansion coefficient and E the ring Young's modulus.

A linear temperature distribution is assumed along the ring radial direction in our work and the resultant thermal moment is given by the following relation:

$$M_t = \frac{1}{12} \alpha_T E b a^2 (\Delta T_{ID} - \Delta T_{OD}) \quad (7)$$

ΔT_{ID} and ΔT_{OD} are the temperature changes at the ring ID and OD respectively.

We have all the necessary equations (5) and (7) to model the thermal moment effect, except that these results are for rectangular cross section rings. For more general geometries as the one presented in Figure 3, we still apply the equations (5) and (7) where we make the approximation of substituting a and b by the following expressions:

$$a = arm + \max(ali, aui) \quad (8)$$

$$b = h_{ui} + a_{ui} \theta_{rt} + h_{li} + a_{li} \theta_{rb} \quad (9)$$

All the geometric variables are presented in Figure 3. θ_{rb} and θ_{rt} are the ring lower and upper flank angles respectively and are assumed to be small enough to apply the first order approximations in equation (9). More details regarding the conformability model development can be found in M.A. Bhouri thesis [37].

Conformability Model Results

In this section, we apply the conformability model to study the effects of bore distortion, gap locations, radial temperature gradient and change of local lubrication conditions.

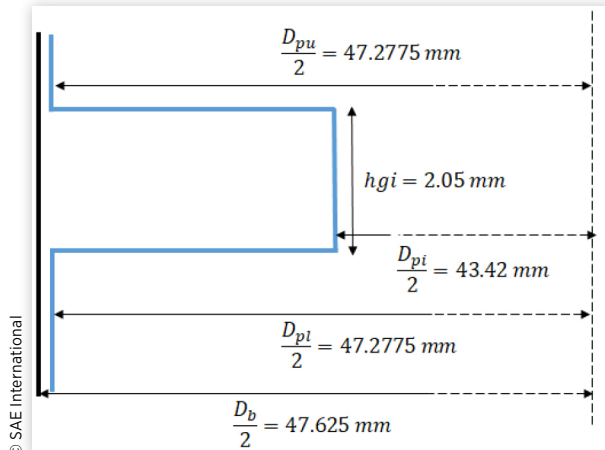
Ring Gap Location Effect Inside Distorted Bore

When the bore experiences thermal and mechanical stresses, it distorts to a non-circular shape with local minimum and maximum radial distances with its initial nominal center. It is customary to describe the geometry of a distorted bore with a discrete Fourier series where a distortion of order 0 corresponds to a change of radius that is uniform along the cylinder circumference due to the expansion of the cylinder when the engine block is heated under operation. Generally, significant cylinder deformation occurs at distortion orders between 0 and 4.

In our simulation, we considered a diesel engine piston whose characteristic dimensions are shown in Figure 4. Studying the effect of non-zero lower and upper flank groove angles for the different studies presented in this paper can be carried out in the future with our ring design tool. We use a ring with a rectangular cross section of dimensions $4\text{ mm} \times 2\text{ mm}$ and a parabolic profile at the running face. The ring has a free shape designed to have uniform pressure distribution at a round shape with a ring tension of 25.4 N . We consider an incoming uniform oil film on the liner with a thickness equal to $5\sigma_p = 1.5\text{ }\mu\text{m}$, where σ_p is the liner surface roughness standard deviation. The oil viscosity is assumed to be the high shear viscosity of a 5 W30 lubricant at 150° C . We consider a liner speed equal to 10 ms^{-1} and directed upward with a zero acceleration. We consider bore distortion up to 4th order: the 0 order amplitude is of order of $100\text{ }\mu\text{m}$, the second one of order of $20\text{ }\mu\text{m}$, the third one of $10\text{ }\mu\text{m}$ and the fourth one of $1\text{ }\mu\text{m}$.

For each of the plots showing the ring deformation in radial coordinates and the radial force distribution, the force is scaled with the maximum value obtained in each case. Based on the location of the ring gap with respect to the cylinder, the ring liner clearance presents different profiles. We refer to the angular position for the ring gap within a fixed coordinate system with respect to the cylinder directed from thrust side (0°) to thrust side (360°). Using that coordinate system, in Figure 5 we plot the radial distance of the distorted bore and the two ring tips. When the gap is located in the vicinity of a cylinder point with a local maximum radial coordinate, the ring is well conforming to the liner as we can see in Figures 5 and 6 and in Figures 7 to 9 for a gap location at

FIGURE 4 Diesel engine characteristic dimensions



© SAE International

FIGURE 5 Ring tips radial coordinates for different ring gap locations

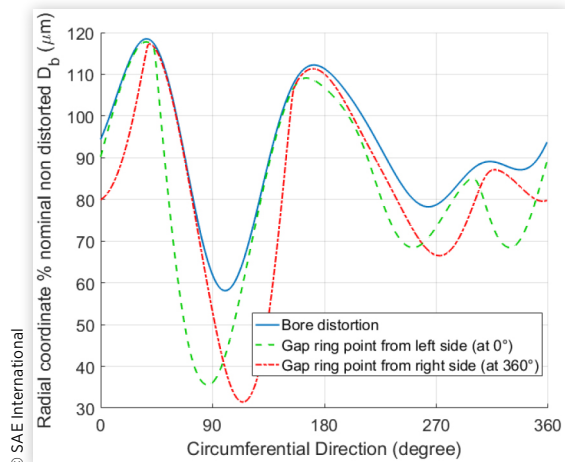


FIGURE 6 Ring tips clearances for different ring gap locations

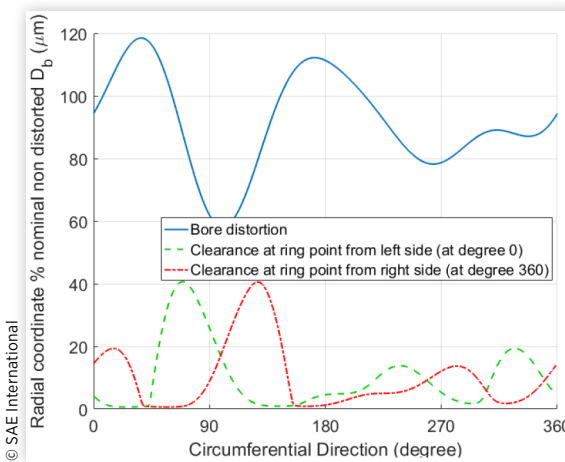


FIGURE 7 Ring and bore in radial coordinate for a gap located at 45°

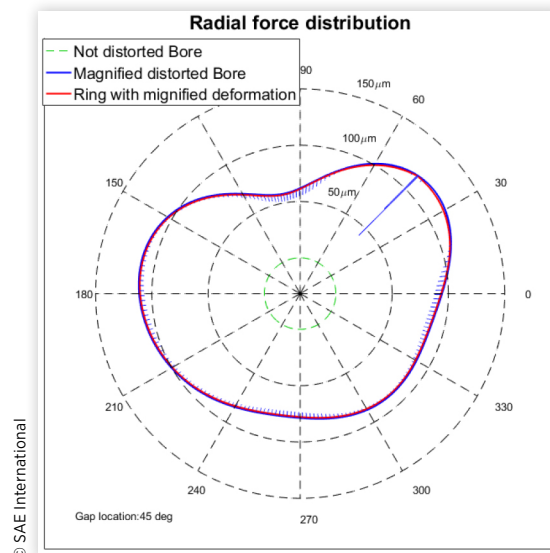
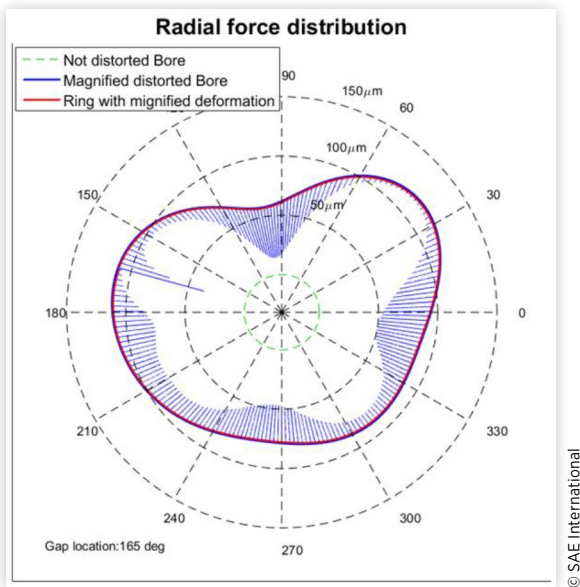
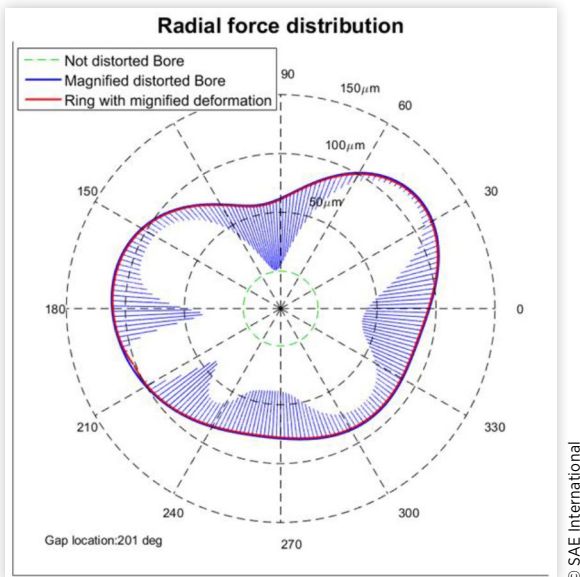


FIGURE 8 Ring and bore in radial coordinate for a gap located at 165°



© SAE International

FIGURE 9 Ring and bore in radial coordinate for a gap located at 201°

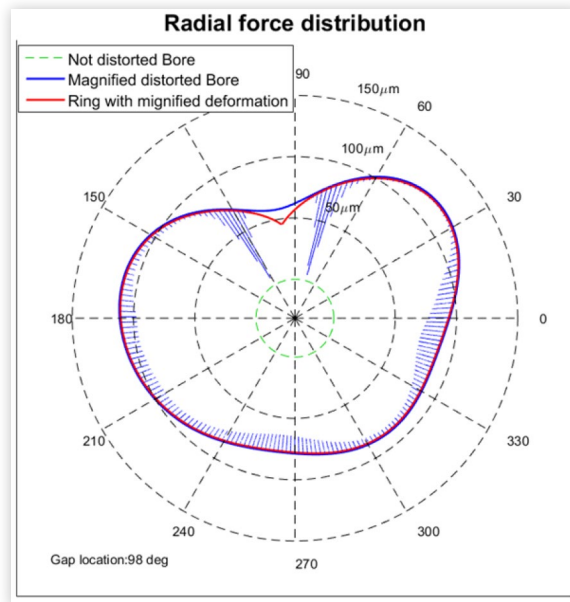


© SAE International

the angles 45°, 165° and 201° respectively with ring-liner clearances less than 1.5 μm , 1.5 μm and 3 μm respectively. For the radial plots we use a magnification coefficient of 1500 for the bore distortion and ring deformation.

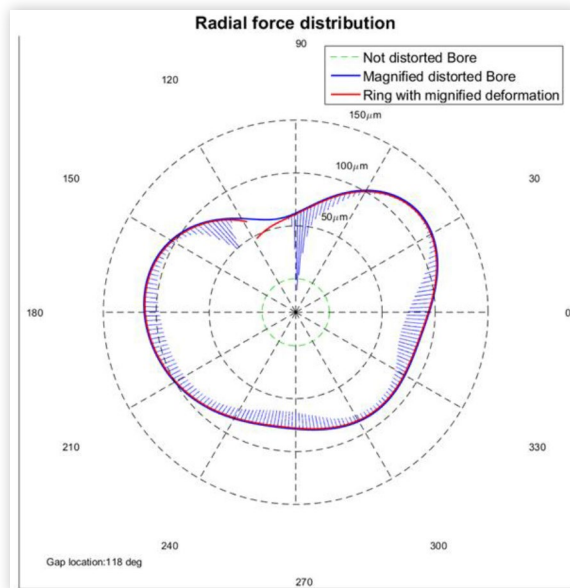
On the other hand, when the ring gap is located in the vicinity of a cylinder point with a local minimum radial coordinate, the ring presents a high clearance with the cylinder since its stiffness does not let it conform well with the local curvature of the cylinder as we can see in Figures 5 and 6 and in Figure 10 and 11 for a gap location at the angles 98° and 118° respectively with maximum ring-liner clearances around 20 μm . For the radial plots we use a magnification coefficient of 1500 for the bore distortion

FIGURE 10 Ring and bore in radial coordinate for a gap located at 98°



© SAE International

FIGURE 11 Ring and bore in radial coordinate for a gap located at 118°



© SAE International

and ring deformation. These clearances compared to the oil film thickness considered of 1.5 μm show very limited oil control performances.

For the rest of this paper, all graphs presenting variables as a function of the circumferential direction are given with respect to a coordinate system defined based on the ring: angles 0° and 360° correspond to the ring tips and 180° corresponds to the ring back. The ring gap static position also affects the radial force distribution. When the ring is not well conforming to the liner, we have larger regions of no-contact. Therefore in these regions, the ring running face is submitted to the gas pressure (the highest among the pressures in the

FIGURE 12 Force distribution comparison for a gap located at 98° and 201°

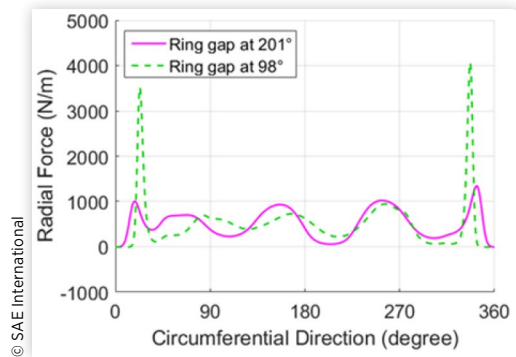
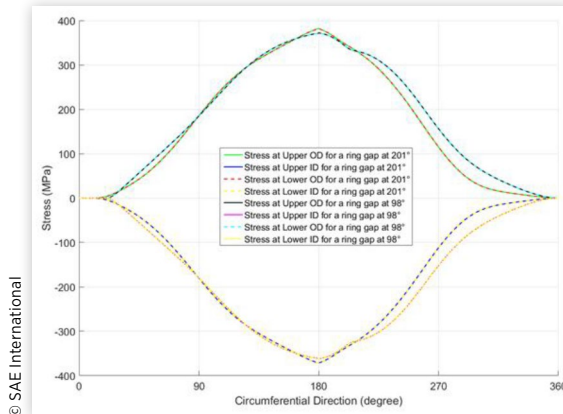


FIGURE 13 Stress distribution comparison for a gap located at 98° and 201°

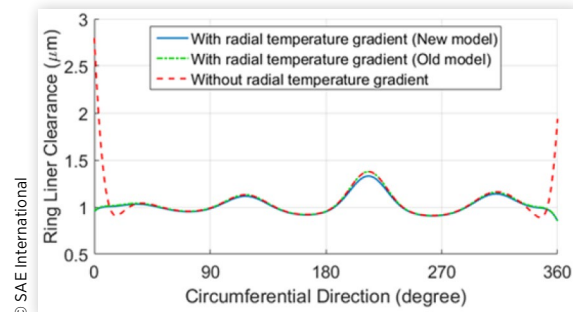


groove upper and lower regions) which is the same as the gas pressure in the inner groove region which is noted by P_i . Therefore, the overall radial force in these regions is zero. However, the average radial force along the ring circumference is almost the same for all the cases corresponding to different ring gap locations and is around the theoretical constant pressure needed to close the ring gap. Therefore, larger no-contact regions mean higher radial force peaks to have the same average value. Thus, for gap location where the ring-liner clearance is high, apart from the oil control issues mentioned previously, we have high local contact forces and thus wear problems. This is confirmed by Figures 12 and 13 where we plotted the radial force and local stress distributions (at upper/lower ID/OD points for each cross section) respectively for the static position obtained when the ring gap is located at 98° (higher clearance and thus higher radial force and higher local stresses) and 201° (lower clearance and thus lower radial force and lower local stresses).

Thermal Moment Effect

In this section we compare the results obtained with our modeling of the thermal moment introduced previously, where we modify the free shape curvature as expressed by

FIGURE 14 Ring-liner clearance with and without radial temperature gradient

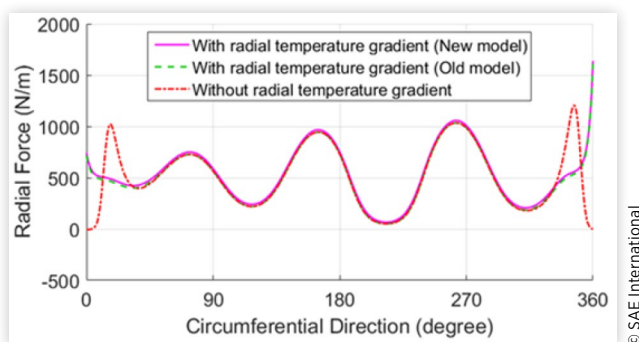


equation (5), and the modeling used by L. Liu [23] where the thermal moment effect is only introduced at the ring tips.

In our simulation, we model the same diesel engine considered in the previous section (Figure 4) with the exact same conditions. The ring gap location is taken equal to 192° so that the ring liner clearance is less than the oil film thickness ($1.5 \mu\text{m}$) along almost the whole ring circumference, which guarantees the ring liner contact and creates the radial temperature gradient. We present the results obtained with the two models for a uniform radial ring temperature gradient equal to 15°C and compare them to the results obtained without radial temperature gradient.

Figure 14 shows the ring liner clearance obtained with the two models. Close to the ring tips the two models give the same results which proves the equivalence between modifying the ring free shape curvature based on the thermal moment and introducing it as an external load. However, the old model only considers the thermal moment effect close to the ring tips. This is a good approximation provided that the ring is well conform to the liner along its whole circumferential direction apart from the tips regions. However, when the ring liner clearance is high enough at any point along the ring circumference, the old model is likely to give biased results as we can see in Figure 14 around the local maximum clearance reached between angles 180° and 270°. In fact, the radial temperature gradient exists all around the ring especially when its clearance with the liner is small enough to have lubrication or dry contact with the liner, which is the case here. Thus, thermal moment effect has to be considered along the whole circumference direction and in particular in the region around the local maximum clearance occurring between 180° and 270°. Indeed, the old model gives exactly the same solution obtained without temperature gradient while our model takes into account the thermal bending moment and gives a lower clearance with the liner. It is true that the difference between the two models in this case is small enough and could be neglected but in some extreme cases where we have high bore distortions and large ring-liner clearances in points far from the ring tips, the thermal moment effect can be significant in those regions and the results obtained with the old model will not be accurate. Besides, computationally our model is slightly more advantageous since we do not have to evaluate the external thermal load at each iteration of the Newton-Raphson algorithm but we just change the free shape curvature and the initial loads accordingly before iterating.

FIGURE 15 Radial force distribution with and without radial temperature gradient



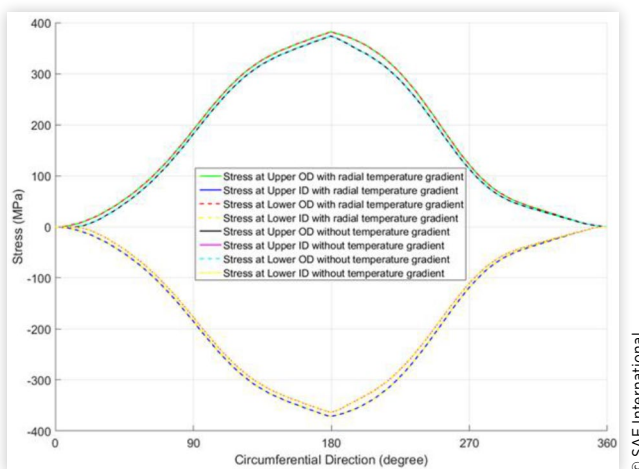
© SAE International

We also verify the results obtained for the radial force distribution given in Figure 15. As expected, since the thermal moment results in a ring expansion decreasing the ring liner clearance, we obtain higher radial force in regions where the clearance has been affected the most which corresponds to points close to the ring tips. Figure 16 gives the stress distributions obtained at the upper/lower ID/OD points of each cross section with the temperature gradient using our new model and without the temperature gradient. Like the radial force distribution, we verify that we have higher stresses (in absolute values) when we have a non-zero temperature gradient. The difference between the two stresses corresponds to the thermal one.

In the rest of this section we keep using the same parameters mentioned previously except for the ring free shape that is no longer designed to have uniform pressure distribution at a round shape with a ring tension of 25.4N but instead we use the TC1 design developed by Mahle and studied by Tomanik [38]. The corresponding free shape and curvature are given in Figure 17.

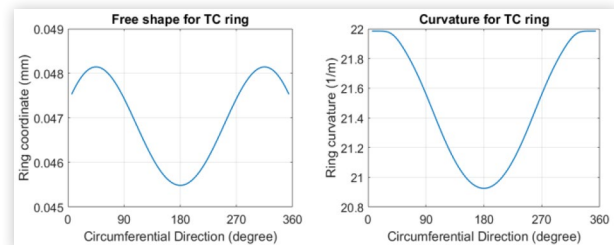
As we can see this ring is designed to have the highest curvature at the tips and a decreasing radial coordinate when we are close to them. This is intended to make the ring clearance higher at the tips and thus decrease the wear effect

FIGURE 16 Stress distributions with and without radial temperature gradient



© SAE International

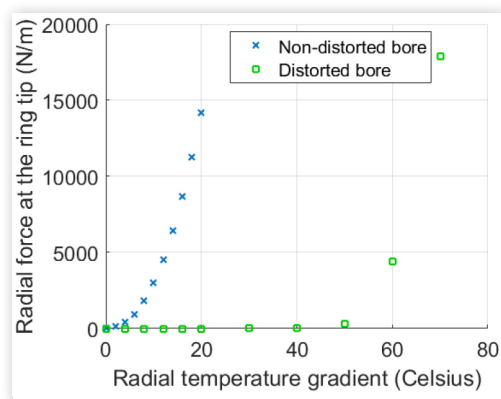
FIGURE 17 TC1 ring free shape and curvature



© SAE International

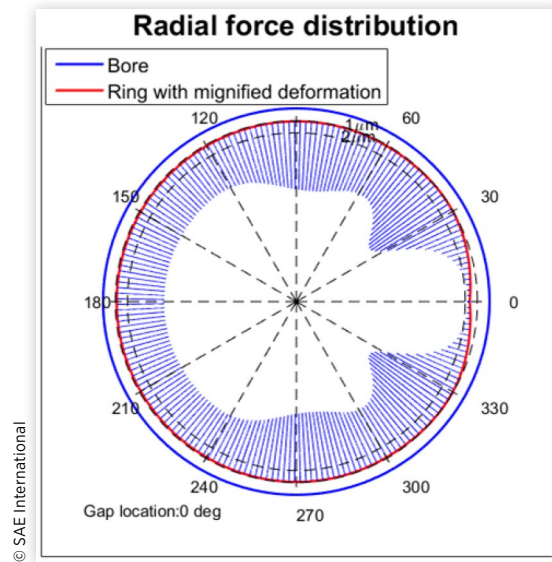
which is maximum in general at these locations. Besides, when experiencing radial temperature gradient, this design is intended to give the ring a shape close to the circular one once inserted in the cylinder. Using the same distorted bore as in the simulations presented above, we verify the performance of this design by looking at the ring-liner clearance and radial force for different temperature gradients. We also simulate the same ring with the same parameters but without bore distortion. For the distorted bore the ring gap is located at the angle 98° as we can see in Figure 21, where the bore distortion and ring deformation are magnified with a coefficient of 3000. This coefficient has also been used for the rest of radial plots given in this section. For that ring tip location, the clearances, and thus the forces generated, at the two ring tips are almost the same. Figure 18 shows the radial force at the ring tip for different radial temperature gradient for the two simulations. As we can see, the TC1 ring does well prevent high force generation at the ring tips when it is inside the distorted bore up to high temperature gradients, around 50°C, since its gap is well located in the vicinity of a cylinder point with a local minimum radial coordinate (here it is a global one) making the clearance at the gap even higher than what is obtained thanks to the ring design, as explained in ring gap location effect study. However, when the ring is inserted in a non-distorted bore, the force generation at the tips increased significantly even for temperature gradients of the order of 8°C. This shows that the TC1 design is well suited to prevent high force generation at the tips, provided it is coupled with bore distortion effects as we can see from Figures 19 and 20

FIGURE 18 Temperature gradient influence on radial force at the ring tip for the TC1 design



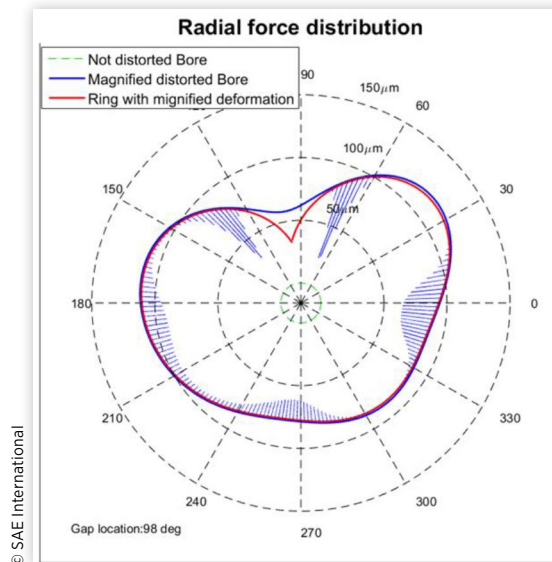
© SAE International

FIGURE 19 Radial plot of the TC1 ring within non-distorted bore and without temperature gradient



© SAE International

FIGURE 20 Radial plot of the TC1 ring within distorted bore and without temperature gradient



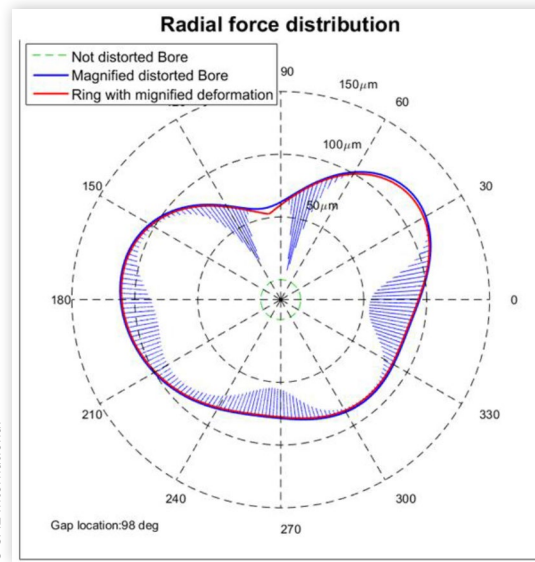
© SAE International

showing the radial plots of the ring without temperature gradient for the two cases.

Nevertheless, we should keep in mind that we are using relatively large cylinder and ring making the thermal effect more significant than what we should obtain for smaller engines. Figure 22 gives the ring-liner clearance at the tip for the same temperature gradients considered in Figure 18 for the two simulations. We can see that the clearance decreases less fast within the distorted bore which is coherent with the observations made for the force generation.

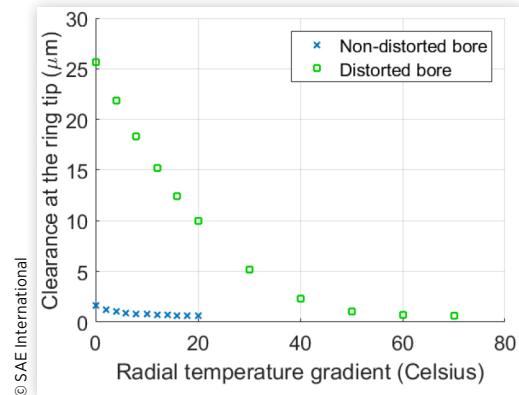
For the non-distorted bore, the clearance without temperature gradient is already small compared to the length scale

FIGURE 21 Radial plot of the ring within distorted bore and with a temperature gradient equal to 30°C



© SAE International

FIGURE 22 Temperature gradient influence on ring-liner clearance at the tip for the TC1 design



of the relative ring-liner clearance generating the contact force. Thus even for small temperature gradient, the force generated at the tips is already high. Figure 19 and 23 give the radial plots of the ring without bore distortion for a zero temperature gradient and a gradient of 6°C respectively. In Figure 23, we see that the tip orientation has already changed unlike the behavior observed in Figure 21 for a higher temperature gradient (30°C) but with a distorted bore.

Figure 24 gives the ring-liner clearance and radial force along the ring circumference for a non-distorted bore with temperature gradients equal to 0°C, 4°C and 6°C, while Figure 25 gives the same plots for a distorted bore with temperature gradients equal to 0°C, 30°C and 60°C. We observe that the non-contact region only exists for the distorted bore case and shrinks when the radial temperature gradient increases till vanishing for a gradient around 50°C, while this non-contact region is nonexistent for the non-distorted bore case. The TC1 design prevents well high force generation at

FIGURE 23 Radial plot of the TC1 ring within non-distorted bore and with a temperature gradient equal to 6°C

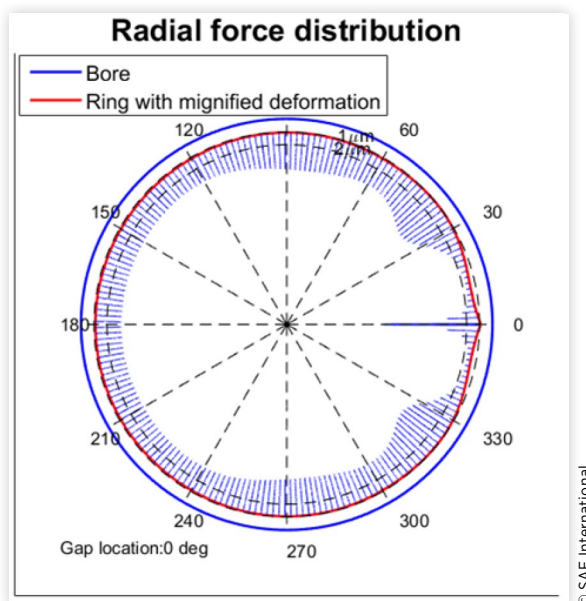


FIGURE 24 Ring-liner clearance and radial force for the TC1 ring within non-distorted bore for different temperature gradients

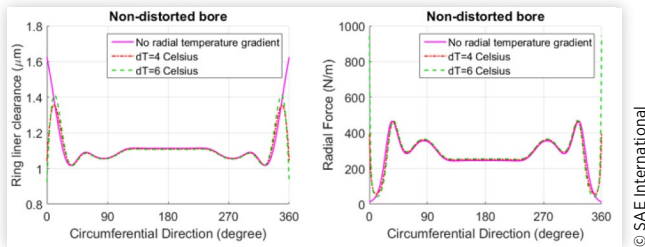
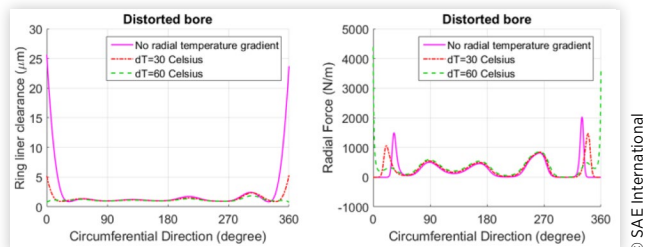


FIGURE 25 Ring-liner clearance and radial force for the TC1 ring within distorted bore for different temperature gradients



the tips when submitted to radial temperature gradients provided the gap is located in the vicinity of a cylinder point with a local minimum radial coordinate. Otherwise the force generation is likely to start even with relatively low temperature gradients, especially for large piston rings.

Oil Accumulation on Liner and Threshold Between Different Lubrication Regimes

The curved beam model is useful in the sense that it relates the global and local behavior of the ring while depending on different length scales. As proven previously, our static model determines the ring structural response under the effect of bore distortion, which represents the global behavior. The local behavior is determined by the response of the ring to different local contact boundary conditions such as bridging and lube-fuel interaction. In this part, we will focus on the ring response to oil accumulation on the liner which affects the global and local behavior of the ring respectively.

In our simulation, we model an engine piston whose characteristic dimensions are shown in Figure 26. We use a ring with a rectangular cross section of dimensions $3\text{ mm} \times 1.5\text{ mm}$ and a parabolic profile at the running face. The free-shape is designed to have uniform pressure distribution at a round shape with a ring tension of 25.4 N . We consider a liner surface roughness standard deviation equal to $\sigma_p = 0.07\text{ } \mu\text{m}$. The oil viscosity is assumed to be the high shear viscosity of a 5 W30 lubricant at 150° C . The gas pressure is taken equal to 1.1 bar in the inner and upper regions of the groove and to 1 bar in the lower one. We use a liner speed equal to 10 m. s^{-1} and directed upward with a zero acceleration. We consider bore distortions up to 4^{th} order with a 0^{th} order distortion of magnitude equal to $80\text{ } \mu\text{m}$, a 2^{nd} order one equal to $10\text{ } \mu\text{m}$ and a 4^{th} one equal to $2\text{ } \mu\text{m}$.

Local oil accumulation on the liner can happen around the bottom dead center during the intake and expansion strokes and around the top dead center during the compression and exhaust strokes and may result in bridging. Inertial and viscous forces bring oil from the piston to the liner causing this local oil accumulation and its range varies from sub-millimeters to tens of millimeters [39] [40] [41] [42]. The trend of the ring-liner and ring-groove contact behavior is mainly determined by the global structural response while the local process makes a difference to the oil supply and contact behavior locally. As shown in the experiments [39] [40], oil film thickness on the liner varies along the circumferential

FIGURE 26 Diesel engine characteristic dimensions (2)

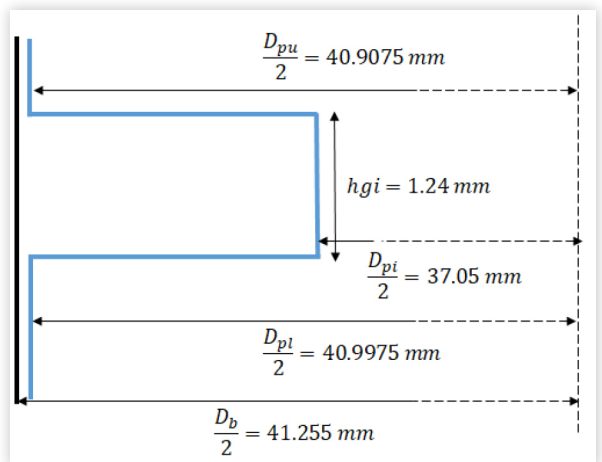
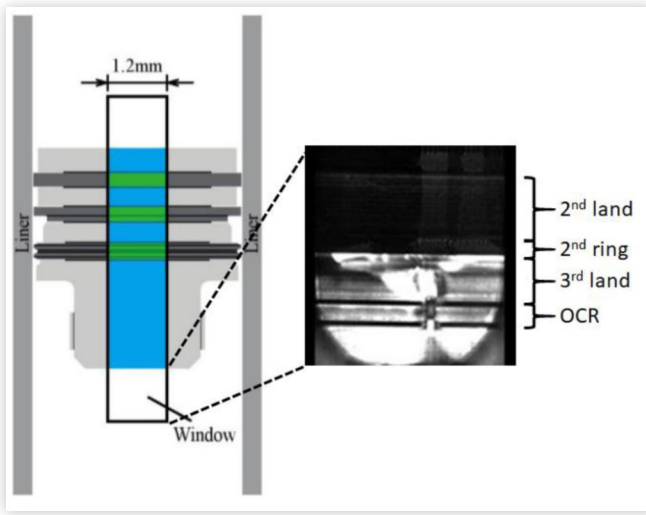


FIGURE 27 Bridging at 650 RPM during compression stroke before TDC (Courtesy of Zanghi)

© SAE International



direction and local oil accumulation is observed. As a result, both of them need to be included to study ring-liner interaction. Bridging mainly occurs at high engine speeds, typically above 3000 RPM. However, Zanghi experimental study [43] shows that bridging can be observed at less than 1500 RPM, at which inertia of the piston is not sufficiently large to drive oil to its top before spreading to the liner. Figure 3 to 12 in [43] shows bridging occurring at 1500 RPM. For coherence, an experimental evidence of bridging at 650 RPM is shown in Figure 27, with generous courtesy of Zanghi. It was taken in a 2D-LIF experiment, which allows an observation of oil distribution through a transparent window in the liner [43, 44], as is shown in Figure 27 (left). Figure 27 (right) was taken slightly before the top dead center (TDC). A brighter color indicates more oil, and a darker color indicates less oil. The bright spots within the piston third land are evidences of bridging. They indicate that oil has been attaching to the liner, which is moving downwards relative to the piston. This shows the contrast between the bridged area and the rest.

In our case we consider a local oil accumulation centered at 90° away from the thrust side, with a width equal 20° . Outside of this accumulation region, oil thickness is fixed to the value of: $2\sigma_p = 0.14 \mu m$ as plotted in Figure 28.

FIGURE 28 Local oil accumulation on the liner for partially flooded case

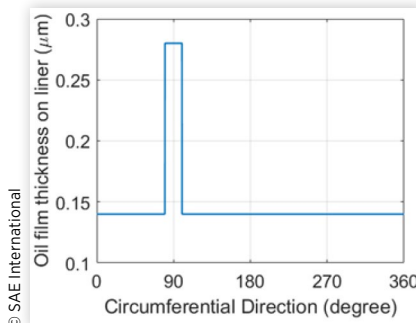
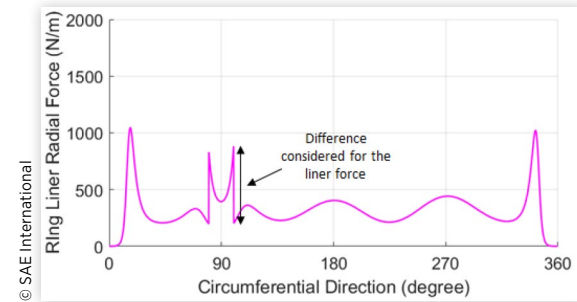


FIGURE 29 Liner force distribution for partially flooded boundary condition



We vary the oil film thicknesses at the peak and change the liner velocity correspondingly to have the same local Reynolds number within the oil accumulation region. Therefore, we can determine the change in the liner force and in the ring-liner clearance depending on the oil film thickness at the peak. We plot the difference between the maximum and minimum of the force distribution within the region where we have the oil accumulation and the maximum ring-liner clearance obtained within that region as function of the difference between the oil film thickness in the accumulation region and the rest of the liner. The difference between the force values is divided by the average of the ring-liner force which is constant here since the gas pressure in the inner region is the same in all the simulation and thus this average value only depends on the ring stiffness, its free shape and the liner surface roughness standard deviation which are all maintained the same. Besides, the difference between the oil film thicknesses and the maximum ring-liner clearance are also made non dimensional by dividing them with respect to the liner surface roughness standard deviation. Figures 29 and 30 show respectively the liner force and the ring-liner clearance obtained with the local oil accumulation corresponding to Figure 28. The variations within these distributions outside the oil accumulation region are mainly due to the bore distortions and the ring free-shape. These results represent a partially flooded case. The tradeoff, defined as a ratio between the oil film thickness and the liner surface roughness standard deviation above which we reach the fully flooded boundary condition, is chosen arbitrarily. In our simulations we fixed it at 10

FIGURE 30 Ring-liner clearance distribution for partially flooded boundary condition

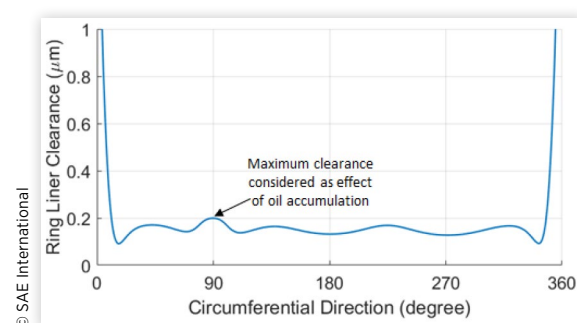


FIGURE 31 Ring-liner clearance and liner force distributions for fully flooded boundary condition

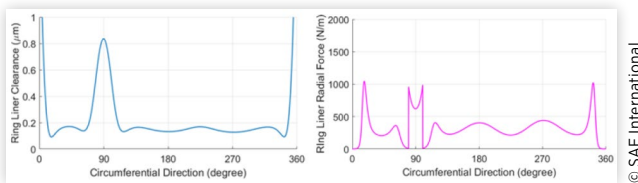
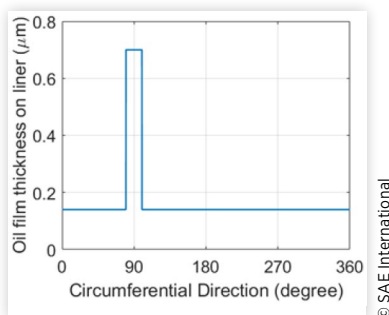


FIGURE 32 Local oil accumulation on the liner for fully flooded case



first. Figure 31 shows the liner force distribution and the ring liner clearance obtained for fully flooded boundary condition within the oil accumulation region corresponding to Figure 32. In this case, the hydrodynamic pressure generation ability of the ring increases compared to the partially flooded case and thus results in a higher ring-liner clearance at the oil peak location. The region where we have the increase in the ring-liner clearance around 90° corresponds to the bridging area. As for the partially flooded case, the discontinuous oil supply generates a discontinuous liner force distribution. Since the dry contact force and hydrodynamic one are very sensitive to the ring-liner clearance at small oil film thickness, we obtain large spikes around the boundary of the bridging area. Because of the stiffness, the ring neutral axis cannot change rapidly. While the ring is able to conform to the bore when we have partially flooded boundary condition, around the bridging area we obtain a narrow range where the ring loses contact with the liner in the fully flooded case. The effect of bridging and local oil accumulation in general remains local and does not affect significantly the ring neutral axis deformation or the liner force distribution outside the oil accumulation region.

Figures 33 and 34 shows the results obtained for the different oil film thicknesses at the peak. We distinguish three regions. The first one is for small peaks where $\frac{\Delta h}{\sigma_p} < 1$, where Δh is the oil film thickness difference between the peak and the rest of the oil film. In this region the resulting force distribution does not depend considerably on the oil film thickness difference. The effect of oil accumulation only emerges starting from $\frac{\Delta h}{\sigma_p} \geq 1$. We observe that the difference introduced for the liner force depends linearly on the oil film thickness difference provided $\frac{\Delta h}{\sigma_p}$ is not big enough. Beyond a certain value $\left(\frac{\Delta h}{\sigma_p}\right)_c$ we start losing the linear dependence. At the same time,

FIGURE 33 Liner force difference with respect to the oil film thickness difference

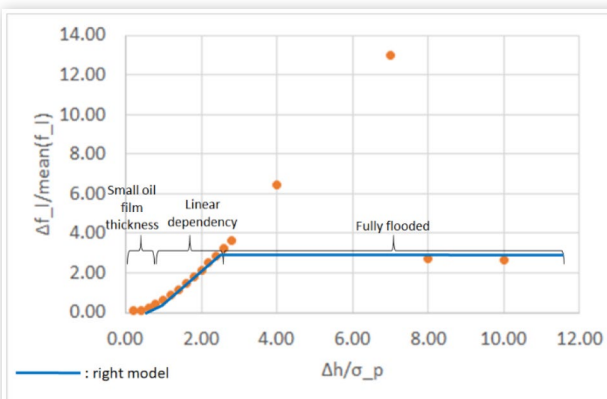
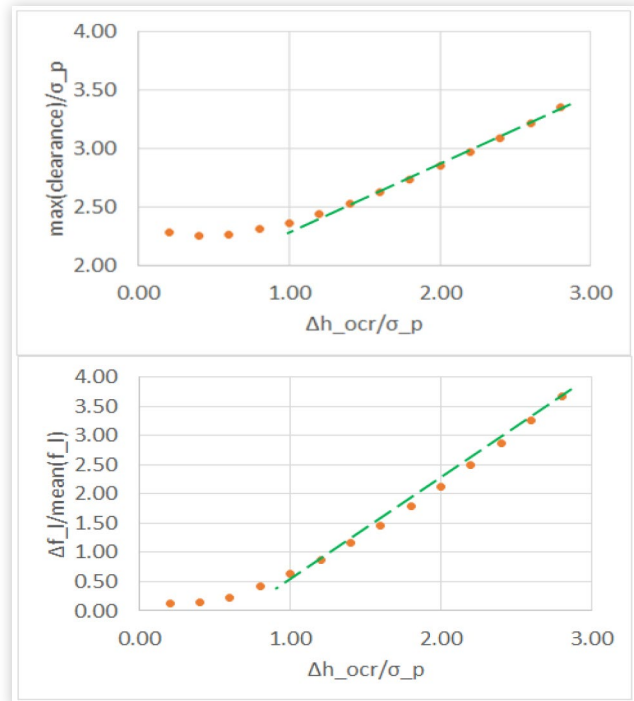


FIGURE 34 Liner force difference and maximum ring-liner clearance with respect to the oil film thickness difference for partially flooded boundary condition at the oil peak



© SAE International

© SAE International

beyond that same value we obtain force distributions those maximum exceed those obtained in the fully flooded case. Therefore, we conclude that our tradeoff to distinguish the partially and fully flooded boundary conditions was over estimated. The more appropriate tradeoff should be $\frac{h_{max} - h_{min}}{\sigma_p} \geq 3$, and since $h_{min} = 2\sigma_p$ we obtain $h_{max} \geq 5\sigma_p$ instead of the 10 chosen arbitrarily at the beginning. Beyond that critical value of $\frac{\Delta h}{\sigma_p}$ we reach the fully flooded boundary condition and the effect of the oil accumulation is independent of the oil film thickness as we can see in Figure 33 for $\frac{\Delta h}{\sigma_p} = 8$ and 10.

In the same manner as for the liner force difference, we also obtain a comparable behavior for the maximum ring-liner clearance at the oil peak location. For $\frac{\Delta h}{\sigma_p} < 1$, the resulting maximum clearance does not vary much with Δh . For $\frac{\Delta h}{\sigma_p} \geq 1$, we obtain again a linear dependence.

When characterizing the effect of oil accumulation, we tried to use non-dimensional variables. The one related to the force difference takes into account the ring tension. The maximum clearance and the oil film thickness difference consider the liner surface roughness standard deviation. The results obtained still depend on the ring stiffness (cross section and Young's modulus) as well as on its free shape. It is also affected by the bore diameter, its distortions and the gas pressure considered. Further analyses are needed if one wants to generalize the effect of these variables on the results that we obtained.

Static Twist under Fixed ID/OD Constraint Model Development

To control gas or oil transport more effectively, top two rings are often designed to have static twist angles after being inserted into the piston and cylinder. This is accomplished by making the ring cross-section asymmetric. The static twist is used in the 2D ring dynamics model [33] that assumes the static twist value is obtained under no external moment. In practice, the static twist is measured by minimizing the external moment as described later. To calculate the static twist, we adapt Liu's method [18] that applies constraints that level the axial position of ring ID or OD depending on the direction of the static twist.

To model the static twist under fixed ID/OD constraint, we use the closing ring method, modify the curved beam finite element model introduced above and consider the appropriate external loads. We also compare the results obtained by our model with the existing straight beam based ring design tool developed by L. Liu.

Experiment Description

To determine the static twist under fixed ID/OD constraint, the ring is first closed such that it has a zero gap. Then, it is introduced within a circular band on a flat plate and the user taps gradually on the ring till it reaches a stable static position. The tapping along the circumferential direction is carried out so that the ring reaches the minimum clearance with the lower plate but without generation of any contact force between them.

Ideally the band would be perfectly circular and the ring gap is zero. However, these two conditions could not be satisfied and our model is able to consider these conditions by introducing band distortion and a non-zero gap. Besides, the tapping process is never carried out such that there is no contact force between the ring and the lower plate. This non-ideal case where the clearance is lower than the one giving a zero force contact can be also modeled with our tool.

FIGURE 35 Ring principle frame, Natural frame and Cylindrical frame

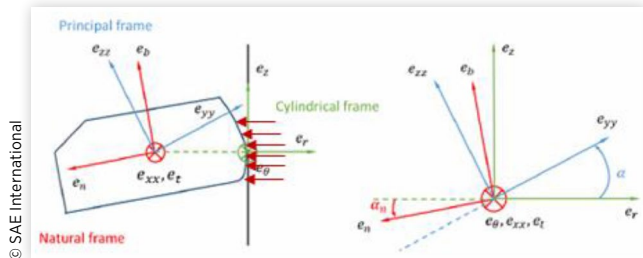
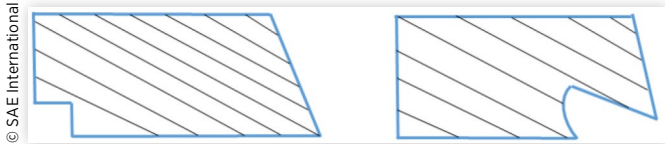


FIGURE 36 Second ring designs



Ring Symmetry

When ring cross section is asymmetric as presented in Figure 35, the principal frame does not align with the natural one creating a non-zero principal angle. When closing the ring to a circular shape and maintaining it in that configuration, we are actually applying a radial load on the outer diameter surface of the ring. Because of the mass distribution within the asymmetric cross section, this radial load creates a local twist moment. Since we are dealing with continuum solid body, the twist of each cross section will create an internal stress applied on the adjacent cross section and makes it twist in the same direction. Thus by moving from each of the ring tips toward the ring back (the opposite point to the tips), we have an increasing total twist moment at each cross section resulting from the internal stress effect plus the radial load applied. This results in an increasing absolute value of the static twist angle which reaches its maximum at the ring back. This explains the numerical and experimental results that we observe for the static twist under fixed ID/OD constraint.

The sign of the static twist depends on the ring cross section and mass distribution. Two types of second rings are shown in Figure 36. The left one is called the scraper ring and the right one the Napier ring. For the second ring, static twist is generally introduced by cutting off the ring material at one of the internal diameter corners. If the ring has a negative principal angle, its static twist will also be negative. In that case, we have a fixed OD constraint. This is the case when the lower internal diameter corner is cut-off. If the ring has a positive principal angle, its static twist will also be positive. In that case we have a fixed ID constraint. This is the case when the upper internal diameter corner is cut-off.

Adaptation of Curved Beam Finite Element Model

In order to adapt the curved beam finite element model for the static twist problem, we keep the modeling of the ring

within the piston and cylinder but only consider dry contact forces introduced in the conformability model for the ring-liner contact which models the ring-band contact and the ring-lower groove dry contact which models the ring-lower plate contact. The ring-upper flank groove contact force will always be zero since we impose the fixed ID/OD constraint which makes the ring in contact with the lower flank groove and adopt a groove clearance bigger than the ring's diagonals which ensures that there is no force generation with the upper groove flank whatever the static twist angle is.

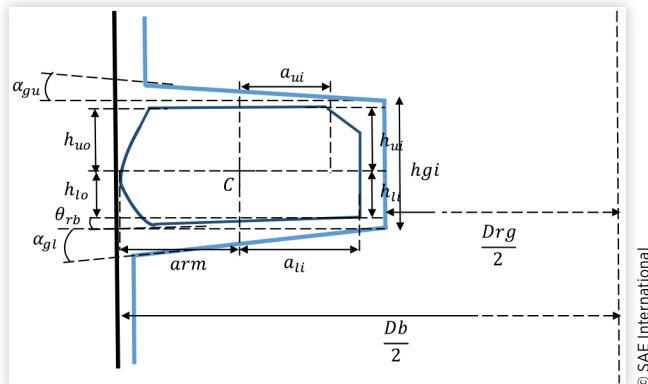
If the ring has a positive principal angle, we apply a fixed ID constraint. This means that the lower internal corner will have the smallest possible clearance with the lower plate, modeled as the groove lower flank, but without the generation of any force contact. Based on the simplified formulation of the greenwood and Tripp pressure contact formula (10) this means that the clearance should be equal to $\Omega\sigma_p$, where $\sigma_p = 0.4 \mu m$ is the standard deviation of the lower plate surface roughness and Ω the threshold that determines the clearance h under which the asperity contact is generated. A typical value for this threshold is 4. If the ring has a negative principal angle, then we apply a fixed OD constraint and it is the lower external corner that will have the smallest possible clearance with the lower plate without the generation of any force contact.

$$P_c = \begin{cases} 0 & \frac{h}{\sigma} \geq \Omega \\ P_k \left(\Omega - \frac{h}{\sigma} \right)^z & \frac{h}{\sigma} \leq \Omega \end{cases} \quad (10)$$

Figure 37 shows the groove and ring-cross section dimensions used to determine the constraint equations to model the fixed ID/Od conditions. These equations will be solved along with Euler-Lagrange equations mentioned previously. D_b and D_{rg} are respectively the bore and groove root diameter. h_{gi} is the groove inner axial height.

The tapping force is modeled as an unknown. In order to keep the same smoothness as the other variables, we interpolate it using 5th order Hermite polynomial spline. Therefore, we add three additional unknowns per node. In order to have a close system, we need to have three equations apart from the Euler-Lagrange ones. Hence, as we do for the axial and radial displacements, we interpolate the angles using the 5th

FIGURE 37 Groove and ring-cross section dimensions



order Hermite polynomial spline so that the constraint gives three additional equations involving the ring coordinates, their first derivatives and the second ones. Hence we give up the 3rd order interpolation for cross section twist adopted in the conformability model.

We model the closing ring process as we carried it out in the conformability study. The axial force f_z in the external vector load includes only the ring-band and ring-lower plate dry contact forces. Euler-Lagrange equations along with the constraint ones give a close system of 24 unknowns and 24 equations per element.

In analogy with the conformability model, we develop the stiffness matrix, load vector and initial force for each element. The different element matrices and vectors are assembled to obtain the finite element equations of the complete ring.

The tapping force is assumed to be applied on the cross section centroid without any offset, thus the tapping force do not contribute to the twist moment term. This is an ideal case but at least minimizes the external twist moment and gives stable results for the two different cases regarding the principal angle sign. More details regarding the Static twist under fixed ID/OD constraint model development can be found in M.A. Bhouri thesis [37].

Sample Results

In this section we compare the results obtained with our model to those given by the existing straight beam model. For all the cases we observe that the absolute value of the static twist is lower for our model. This shows an advantage of adopting the curved beam model compared to the straight beam one, since it solves for a stability position with a lower static twist and thus a lower twist moment which is the intuition behind the static twist under fixed ID/OD constraint experiment. In fact, the users try to figure out the stability position of the ring when it is closed to a circular shape with the minimum possible static twist. This explains the gradually increasing tapping force adopted in order to minimize the clearance with the lower stage but without introducing any force contact with it or any additional twist moment.

Figures 38 and 39 show that the bigger the cut off engineered on the ring, the larger the absolute value of the static twist angle is. In fact, for a larger cut off, the local twist moment distribution along the axial axis introduced by the

FIGURE 38 Ring cross section with a 0.5 x 0.5 mm cut off on the internal upper corner of a 2 x 4 mm ring and the corresponding twist angle

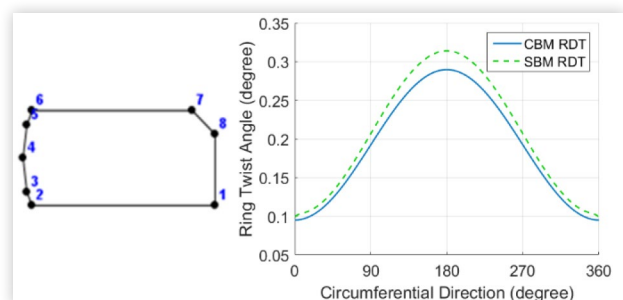


FIGURE 39 Ring cross section with a 0.2×0.2 mm cut off on the internal upper corner of a 2×4 mm ring and the corresponding twist angle

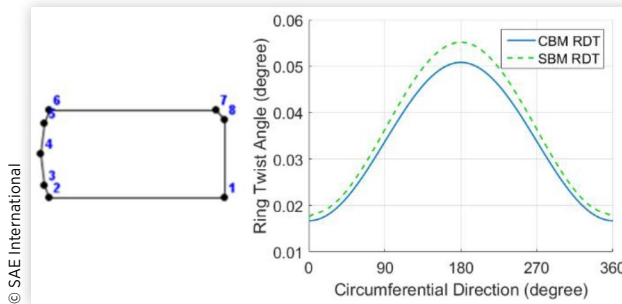
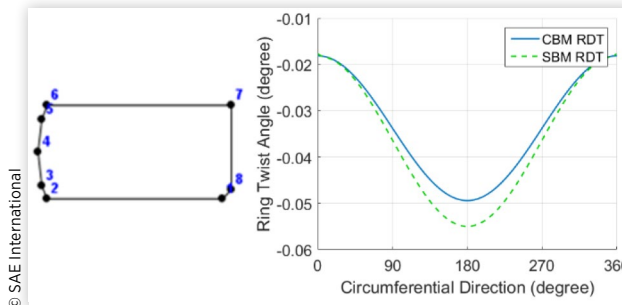


FIGURE 40 Ring cross section with a 0.2×0.2 mm cut off on the internal lower corner of a 2×4 mm ring and the corresponding twist angle



radial force is bigger, since the mass distribution varies in a wider range. Therefore, the resulting static twist angle is bigger in absolute value.

Figures 39 and 40 show the almost symmetric results for the symmetric cut offs realized on the ring. The small discrepancy in the symmetry for the results obtained for the twist angle is due to the fact that the ring of Figure 39 with a positive twist and a minimum clearance at the internal lower corner is not symmetric to the case of the ring in Figure 40 with a negative twist and a minimum clearance at the external lower corner. Indeed, the centroid radial position is the same for these two rings but since the minimum clearance constraint is once applied on the internal lower corner and once on the external one, the twist angles needed will not be the opposite of each other, because the distances between each of these points where we have the constraint and the centroid is not the same.

Figures 41 and 42 show the results obtained for rings with non-zero upper or lower flank angles. Again these two cases are not exactly symmetric since the radial distance between the centroid and the lower corner points where we have the constraint in each case is not the same: ali for the case of Figure 41 is different from alo of the ring in Figure 42. Therefore the constraints are not symmetric for opposite α , and hence we do not obtain perfectly opposite static twist angles.

FIGURE 41 Ring cross section with a cut off along the upper flank of a 2×4 mm ring and the corresponding twist angle

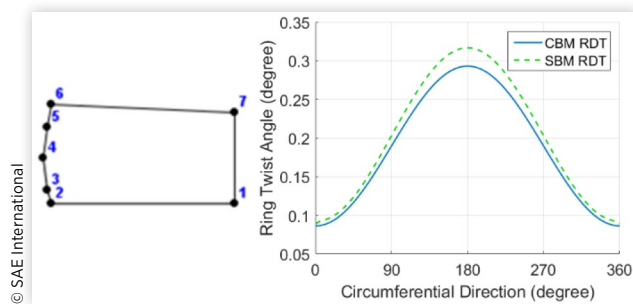
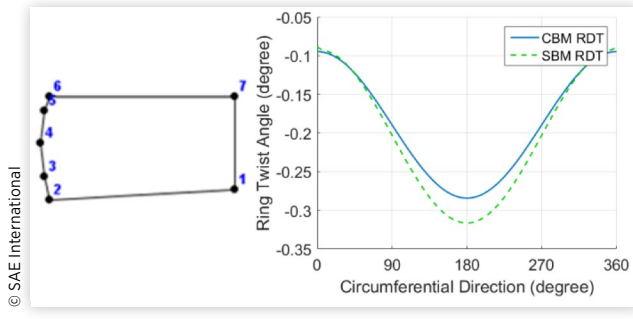


FIGURE 42 Ring cross section with a cut off along the lower flank of a 2×4 mm ring and the corresponding twist angle



Conclusions

The dual grid curved beam based model is an appropriate approach for the interaction of the ring and bore as well as ring and groove. The way the model is set up allows one to not only carry out conventional conformability studies but also much of the real running conditions in an engine cycle. In particular, we looked at the effect of the radial temperature gradient and showed that our model generalizes the existing one by considering the bending moment along the whole ring and not restricting it at the tips. Relating the global and local behaviors of the ring, we analyzed the effect of the ring gap location within a distorted bore on the ring-liner conformability. Ring structural response also depends on local oil distribution on the liner. In particular, we quantified the threshold that should be used to distinguish between the two lubrication boundary conditions. The same analysis characterizes the ring response to local oil accumulation or bridging.

We extended the curved beam model based on nodal displacements to determine the static twist under fixed ID/OD by simulating the axial taping force carried out in the experimental set-up. A physical understanding of the generation of the static twist from the radial pressure was given and a study of the ring's asymmetry effect along with sample results were presented. Besides, developing a static twist under fixed ID/OD constraint based on curved beam model is

essential to conceive a complete ring design tool based solely on that modelling that allows us to reach a better accuracy with less computation cost than the straight beam model. This tool is of practical interest for ring designers to have an analytical tool that determines the ring static twist based on its design which will facilitate the iterative design process needed to obtain the desired static twist.

The ring conformability is crucial for the ring pack performances in terms of gas sealing and oil consumption. We used our model to analyze ring structural responses to different global and local conditions. Further analyzes based on dimensionless number need to be carried out in order to relate these behaviors in a more general frame work. For instance, the results giving the threshold between the two lubrication boundary conditions on the liner could be improved by looking at the effect of the ring stiffness (cross section and Young's modulus), its free shape, the bore diameter, its distortions and the gas pressures on the results obtained. Moreover, our model could be extended to quantify the amount of oil that is scraped because of bridging and determine the effective parameters that determine it. In addition, the whole conformability model could be upgraded by modelling the ring tips overlapping. This upgrading can also be applied to the static twist under fixed ID/OD constraint model.

References

1. Tian, T., "Dynamic Behaviors of Piston Rings and their Practical Impact. Part 1: Ring Flutter and Ring Collapse and their Effects on Gas Flow and Oil Transport," *Proceedings of IMechE, Part J: Journal of Engineering Tribology* 216:209-227, 2002.
2. Tian, T., "Dynamic Behaviors of Piston Rings and their Practical Impact. Part 2: Oil Transport, Friction, and Wear of Ring/Liner Interface and the Effects of Piston and Ring Dynamics," *Proceedings of IMechE, Part J: Journal of Engineering Tribology* 216:229-247, 2002.
3. Timoshenko, S. and Lessells, J.M., "Applied Elasticity," (East Pittsburgh, Westinghouse Press, 1925).
4. Sun, D.C., "A Thermal Elastica Theory of Piston-Ring and Cylinder-Bore Contact," *ASME Journal of Applied Mechanics* 58:141-153, 1991.
5. E. W. Schneider, D. H. Blossfeld, D. C. Lechman, R. F. Hill, R. F. Reising, and J. E. Brevick, "Effect of Cylinder Bore out-of-Roundness on Piston Ring Rotation and Engine Oil Consumption," *SAE Technical Paper 930796*, 1993, doi:[10.4271/930796](https://doi.org/10.4271/930796).
6. Hitosugi, H., Nagoshi, K., Komada, M., and Furuhama, S., "Study on Mechanism of Lubricating Oil Consumption Caused by Cylinder Bore Deformation," *Internal Combustion Engines* 2015:06-22, 1996.
7. Hitosugi, H., Nagoshi, K., Ebina, M., and Furuhama, S., "Study on Cylinder Bore Deformation of Dry Liner in Engine Operation," *JSAE Review* 17(2):113-119, 1996.
8. R. Müller, "Zur Frage des Formfüllungsvermögen von Kolbenringen in von der Kreisform abweichenden Bohrungen gleicher Umfangslänge," *MTZ*, vol. 31, pp. 79-82, 1970.
9. Dunaevsky, V.V., "Analysis of Distortions of Cylinders and Conformability of Piston Rings," *Tribology Transactions* 33(1):33-40, 1990.
10. Dunaevsky, V., Alexandrov, S., Barlat, F., 2000, "Analysis of Three-Dimensional Distortions of the Piston Rings with Arbitrary Cross-Section," *SAE Paper 2000-01-3453*, doi:[10.4271/2000-01-3453](https://doi.org/10.4271/2000-01-3453).
11. Dunaevsky, V.V., Alexandrov, S., and Barlat, F., "Fundamentals for analysis of threedimensional distortions of the piston rings." . In: *Proceedings of the 2000 Fall Technical Conference of the ASME Internal Combustion Engine Division*. (2000), 15-22.
12. V. V. Dunaevsky, "Development of Conformability Model of Piston Rings with Consideration of their Three-dimensional Torsional Distortions and Fourier Series Representation of Cylinder Bore Geometry," in *SAE Technical Paper 2002-01-3131*, 2002, doi:[10.4271/2002-01-3131](https://doi.org/10.4271/2002-01-3131).
13. Dunaevsky, V. and Rudzitis, J., "Clarification of a Semi-Empirical Approach in Piston Ring-Cylinder Bore Conformability Prediction," *Journal of Tribology* 129(2):430, 2007.
14. Tomanik, E., "Piston Ring Conformability in a Distorted Bore," *SAE Transactions* 105(5):394-405, 1996.
15. E. Tomanik, "Improved Criterion for Ring Conformability Under Realistic Bore Deformation," in *SAE Technical Paper 2009-01-0190*, 2009, doi:[10.4271/2009-01-0190](https://doi.org/10.4271/2009-01-0190).
16. Ma, J., Ryan, T. W., Winter, J., and Dixon, R., 1996, "The Piston Ring Shape and its Effects on Engine Performance," *SAE Paper 960052*, doi:[10.4271/960052](https://doi.org/10.4271/960052).
17. M. A. Ejakov, H. J. Schock, and L. J. Brombolich, "Modeling of Ring Twist For an IC Engine," in *SAE Technical Paper 982693*, 1998, doi:[10.4271/982693](https://doi.org/10.4271/982693).
18. L. Liu, T. Tian, and R. Rabuté, "Development and Applications of an Analytical Tool for Piston Ring Design," in *SAE Technical Paper 2003-01-3112*, 2003, doi:[10.4271/2003-01-3112](https://doi.org/10.4271/2003-01-3112).
19. L. Liu and T. Tian, "A Three-Dimensional Model for Piston Ring-Pack Dynamics and Blow-By Gas Flow," in *ASME 2004 Internal Combustion Engine Division Fall Technical Conference ICEF2004-0968*, 2004.
20. L. Liu and T. Tian, "Modeling Piston Ring-Pack Lubrication With Consideration of Ring Structural Response," *SAE International*, Warrendale, PA, 2005-01-1641, Apr. 2005, doi:[10.4271/2005-01-1641](https://doi.org/10.4271/2005-01-1641).
21. Prescott, J., "Applied Elasticity," (New York, Dover Publication Inc, 1925).
22. Dunaevsky, V., Alexandrov, S., and Barlat, F., "The Effect of Contact Pressure on Piston Ring Twist," *SAE Paper 2001-01-2720*, 2001, doi:[10.4271/2001-01-2720](https://doi.org/10.4271/2001-01-2720).
23. L. Liu, " Modeling the Performance of the Piston Ring-Pack with Consideration of Non-Axisymmetric Characteristics of the Power cylinder System in Internal Combustion Engines," Ph.D. Thesis, the Department of Mechanical Engineering, Massachusetts Institute of Technology, Cambridge, MA, 2005.
24. C. Baelden, "A Multi-scale Model for Piston Ring Dynamics, Lubrication and Oil Transport in Internal Combustion Engines," Ph.D. Thesis, the Department of Mechanical

- Engineering, Massachusetts Institute of Technology, Cambridge, MA, 2014.
25. Baelden, C. and Tian, T., "A Dual Grid Curved Beam Finite Element Model of Piston Rings for Improved Contact Capabilities," *SAE Int. J. Engines* 7(1), 2014, doi:[10.4271/2014-01-1085](https://doi.org/10.4271/2014-01-1085).
 26. Y. Liu "A Multi-scale Model Integrating both Global Ring Pack Behavior and Local Oil Transport in Internal Combustion Engines," Ph.D. Thesis, the Department of Mechanical Engineering, Massachusetts Institute of Technology, Cambridge, MA, 2017.
 27. Liu, Y. and Tian, T., "Development and Application of Ring-Pack Model Integrating Global and Local Processes. Part 1: Gas Pressure and Dynamic Behavior of Piston Ring Pack," *SAE Int. J. Engines* 10(4), 2017, doi:[10.4271/2017-01-1043](https://doi.org/10.4271/2017-01-1043).
 28. Liu, Y., Li, Y., and Tian, T., "Development and Application of Ring-Pack Model Integrating Global and Local Processes. Part 2: Ring-Liner Lubrication," *SAE Int. J. Engines* 10(4), 2017, doi:[10.4271/2017-01-1047](https://doi.org/10.4271/2017-01-1047).
 29. Greenwood, J.A. and Tripp, J.H., "The Contact of two Nominally Flat Rough Surfaces," *Proceedings of the Institution of Mechanical Engineers* 185(1):625-633, 1970.
 30. Hu, Y., Cheng, H.S., Arai, T., Kobayashi, Y., and Aoyama, S., "Numerical Simulation of Piston Ring in Mixed Lubrication - A Nonaxisymmetrical Analysis," *ASME Journal of Tribology* 116(3):470-478, 1994.
 31. H. Chen, "Modeling the lubrication of the piston ring pack in internal combustion engines using the deterministic method," Ph.D. Thesis, the Department of Mechanical Engineering, Massachusetts Institute of Technology, Cambridge, MA, 2011.
 32. H. Chen, Y. Li and T. Tian, "A novel approach to model the lubrication and friction between the twin-land oil control ring and liner with consideration of micro structure of the liner surface finish in internal combustion engines," *SAE Technical Paper*, no. [2008-01-1613](https://doi.org/10.4271/2008-01-1613), 2008, doi:[10.4271/2008-01-1613](https://doi.org/10.4271/2008-01-1613).
 33. T. Tian, "Modeling the Performance of the Piston Ring-Pack in Internal Combustion Engines," Ph.D. Thesis, the Department of Mechanical Engineering, Massachusetts Institute of Technology, Cambridge, MA, 1997.
 34. Tian, T., Noordzij, L.B., Wong, V.W., and Heywood, J.B., "Modeling Piston-Ring Dynamics, Blowby, and Ring-Twist Effects," *ASME Transaction - Journal of Engineering for Gas Turbines and Power* 120:849-854, 1998.
 35. Cheng, C., Kharazmi, A., Schock, H., Wineland, R., and Brombolich, L., "Three-Dimensional Piston Ring-Cylinder Bore Contact Modeling," *ASME. Journal of Engineering for Gas Turbines and Power* 137(11):111505-111505-10, 2015, doi:[10.1115/1.4030349](https://doi.org/10.1115/1.4030349).
 36. Mierbach, A., Duck, G. E., and Newman, B. A., 1983, "Heat Flow through Piston Rings and its Influence on Shape," *SAE Paper* [831283](https://doi.org/10.4271/831283), doi:[10.4271/831283](https://doi.org/10.4271/831283).
 37. Bhouri, M.A., "Curved beam based model for piston-ring designs in internal combustion engines," M.S. Thesis, the Department of Mechanical Engineering, Massachusetts Institute of Technology, Cambridge, MA, 2017.
 38. Tomanik, E. and Bruno, R., "Calculation of Piston Ring Radial Pressure Distribution from its Measured Free Shape," *SAE Technical Paper* [2012-01-1322](https://doi.org/10.4271/2012-01-1322), 2012, doi:[10.4271/2012-01-1322](https://doi.org/10.4271/2012-01-1322).
 39. S. S. V. Przesmitzki, "Characterization of oil Transport in the Power Cylinder of Internal Combustion Engines During Steady State and Transient Operation," Ph.D. Thesis, the Department of Mechanical Engineering, Massachusetts Institute of Technology, Cambridge, MA, 2008
 40. E. B. Senzer, "Oil Transport Inside the Oil Control Ring Grove and its Interaction with Surrounding Areas in Internal Combustion Engines," Ph.D. Thesis, the Department of Mechanical Engineering, Massachusetts Institute of Technology, Cambridge, MA, 2012.
 41. T. Fang, "Computations and Modeling of Oil Transport between Piston Lands and Liner in Internal Combustion Engines," Master Thesis, the Department of Mechanical Engineering, Massachusetts Institute of Technology, Cambridge, MA, 2014.
 42. S. Przesmitzki, A. Vokac and T. Tian, "An Experimental Study of Oil Transport between the Piston Ring Pack and Cylinder Liner," *SAE Technical Paper*, no. [2005-01-3823](https://doi.org/10.4271/2005-01-3823), 2005, doi:[10.4271/2005-01-3823](https://doi.org/10.4271/2005-01-3823).
 43. Zanghi, E. J., "Analysis of Oil Flow Mechanisms in Internal Combustion Engines Via High Speed Laser Induced Fluorescence (LIF) Spectroscopy," Master's thesis, Department of Mechanical Engineering, Massachusetts Institute of Technology, Cambridge, MA, 2014.
 44. Thirouard, B., "Characterization and modeling of the fundamental aspects of oil transport in the piston ring pack of internal combustion engines," Ph.D. thesis, Department of Mechanical Engineering, Massachusetts Institute of Technology, Cambridge, MA, 2001.

Acknowledgments

This work has been sponsored by the MIT consortium on Lubrication in Internal Combustion Engines with additional support from Argonne National Laboratory and the US Department of Energy. The authors would like to thank all current members: Daimler AG, Mahle GmbH, MTU Friedrichshafen, PSA Peugeot Citroën, Renault S.A., Royal Dutch Shell, Toyota, Volkswagen AG, Volvo Cars, Volvo Truck, and Weichai Power.